SUPERSONIC TURBINE DESIGN AND PERFORMANCE

Louis J. Goldman
National Aeronautics and Space Administration
Lewis Research Center
Cleveland, Ohio

ABSTRACT

Methods for designing supersonic stator and rotor blading corrected for boundary layer displacement thickness are summarized. Computer programs based on these methods have been reported in NASA publications. Analytical blade losses for blading of this type are presented and design limitations resulting from consideration of flow separation and supersonic starting are discussed. In addition, a summary of the experimental performance of a single-stage turbine designed by these methods is given.

INTRODUCTION

A supersonic turbine stage is one in which the absolute velocity at the nozzle exit and the relative velocity at rotor inlet are supersonic. Supersonic turbines have potential application in turbopump and open-cycle auxiliary power systems (1)[1], where high-energy fluids are used and high pressure ratios are available. In addition, their use in high temperature turbo-engines for primary propulsion systems has recently been proposed (2). This interest in supersonic turbines has created a need for both analytical design methods and experimental data for this type of turbine.

Computer programs for the design of supersonic turbine blading have been described in (3,4). The stator blading consists of sharp-edged throat nozzles designed to produce uniform parallel flow at the blade exit. The rotor blading is designed to produce a blade-to-blade free-vortex flow within the passage. Blade losses are accounted for analytically in the design procedure by correcting the ideal profiles for boundary layer displacement thickness. Losses due to mixing the flow to uniform conditions downstream of the blades are considered in the design method. However, other blade losses, such as shock formation or flow separation that may occur in an actual turbine are not accounted for.

The experimental performance of a single-stage partial-admission supersonic turbine designed by these methods has been recently reported in (5). The turbine was tested over a range of pressure ratios from 20 to 150 and equivalent speeds from 20 to 100 percent of design.

This paper summarizes both the analytical design procedure and the experimental results obtained. The analytical loss characteristics for typical stator and rotor blading are also presented. In addition, the design limitations imposed by consideration of flow separation, blade solidity, and supersonic starting problems are discussed.

[1]Numbers underlined in parentheses designate references at end of paper.

SYMBOLS

a	speed of sound, m/sec (ft/sec)
C	blade chord, m (ft)
C_p	specific heat at constant pressure, J/(kg)(K) (Btu/(lb)(^oR))
G	blade spacing, m (ft)
H_i	incompressible form factor
h	specific enthalpy, J/kg (Btu/lb)
I	moment of inertia, N-m-sec^2 (ft-lb-sec^2)
M	Mach number
m	slope of speed versus time curve, rad/sec^2
p	pressure, N/m^2 (lb/ft^2)
R	radius of turbine, m (ft)
Re	Reynolds number, $w/\mu_o R$
Re_R	rotor Reynolds number, $\rho'_{r,2} C W_2/\mu'_2$
Re_t	nozzle throat Reynolds number, $\rho_o y_t \dot{V}_t/\mu_o$
T	temperature, K (^oR)
t	time, sec
U	blade speed, m/sec (ft/sec)
V	velocity, m/sec (ft/sec)
V_j	velocity corresponding to isentropic expansion from inlet total pressure to exit static pressure, $\sqrt{2\Delta h_{id}}$, m/sec (ft/sec)
W	relative velocity, m/sec (ft/sec)
w	mass-flow rate, kg/sec (lb/sec)
y	width, m (ft)

TM X-67961

α nozzle flow angle from axial direction, deg

γ specific heat ratio

γ^* specific heat ratio at U.S. standard conditions, 1.4

δ p_o'/p^*

ε gamma function, $\frac{\gamma^*}{\gamma}\left\{\frac{\left(\frac{\gamma+1}{2}\right)^{\gamma/\gamma-1}}{\left(\frac{\gamma^*+1}{2}\right)^{\gamma^*/\gamma^*-1}}\right\}$

η blade efficiency

η_s turbine static efficiency

θ_{cr} $(V_{cr}/V_{cr}^*)^2$

μ coefficient of viscosity, kg/(m)(sec) (lb/(ft)(sec))

ν blade-jet speed ratio, U_m/V_j

ρ density, kg/m^3 (lb/ft^3)

σ blade solidity, C/G

τ torque, N-m (ft-lb)

ω rotative speed, rad/sec

Subscripts:

acc acceleration

cr critical

dec deceleration

f full admission

fs free-stream

id ideal

ℓ lower surface

m mean

n nozzle or stator

R rotor

r relative to rotor

t nozzle throat

u upper surface

x axial

0 stator inlet

1 stator exit

2 stator aftermixing state (also rotor inlet)

3 rotor exit

4 rotor aftermixing state

Superscripts:

' total conditions

* U.S. standard conditions

TURBINE DESIGN

The design of both the stator and rotor blading is accomplished in a similar manner. First, the ideal passage (stator or rotor) is designed by the method of characteristics as applied to the isentropic flow of a perfect gas. Boundary layer parameters are then calculated for the ideal passage and the final profile is obtained by correcting the ideal profile for the displacement thickness. A stator and a rotor designed in this manner are shown in figures 1 and 2, respectively.

Stator Blades

The design of the ideal stator blading is based on establishing uniform parallel flow at the blade exit in the minimum possible distance. The computer program described in (6) is used for this purpose. A typical sharp-edged-throat nozzle of this type (shown in fig. 1) consists of three sections: (1) a converging section, (2) a diverging section, and (3) a straight section. The converging section produces the flow turning with small losses and is not designed by the computer program. The symmetric diverging section accelerates the flow to the desired free-stream Mach number at the blade exit. The straight line segment, parallel to the flow direction, completes the nozzle profile.

The boundary layer parameters (displacement and momentum thicknesses) are calculated using the computer program described in (7). The program uses Cohen and Reshotko's method (8) for laminar boundary layers and Sasman and Cresci's method (9) for turbulent boundary layers. Curvature effects are not considered in these methods. For flows in highly favorable pressure gradients, as occur in the stator, the laminar results are extrapolated by the method described in (8). Transition from laminar to turbulent flow, if it occurs, is predicted by the program, or the user may force transition at any station in the nozzle.

A complete description of the computer program for the design of supersonic nozzles corrected for boundary layer displacement thickness is given in (3). The program input consists primarily of the nozzle exit Mach number, nozzle angle, specific heat ratio, and total flow conditions. The program output gives the corrected nozzle profile.

Rotor Blades

The design of the ideal rotor blading is based on establishing vortex flow within the blade passage by a procedure similar to that described in (10). The computer program described in (11), based on this procedure, is used for the calculation of the ideal passage. A typical passage (shown in fig. 2) consists essentially of three major parts: (1) inlet transition arcs, (2) circular arcs, and (3) outlet transition arcs. The inlet transition arcs (upper and lower surfaces) are required to convert the uniform parallel flow at the passage inlet into vortex flow. The concentric circular arcs turn and maintain the vortex flow condition. The outlet arcs reconvert the vortex flow into uniform parallel flow at the

passage exit. Straight line segments, on the suction surface, parallel to the inlet and outlet flow directions complete the passage.

The ideal rotor passage is designed so that the outlet spacing is less than the inlet spacing (see fig. 2). This is necessary since it is required that the ideal passage corrected for boundary layer displacement thickness have equal inlet and outlet spacings. For an ideal passage designed for equal inlet and outlet Mach numbers, this is accomplished by having less circular turning for the outlet portion of the passage than for the inlet portion. An iterative procedure is required to determine the circular turning necessary to give equal spacings.

A complete description of the computer program for the design of supersonic rotor blades corrected for boundary layer displacement thickness has been given in (4). The program input consists essentially of the inlet and exit Mach numbers, flow angles, specific heat ratio, circular arc Mach numbers, and total flow conditions. The program output consists of the corrected rotor passage and the boundary layer parameters.

A number of input options related to the boundary layer calculations are also available to the user. For laminar boundary layers the program will generally predict separation in the rotor for fairly small adverse pressure gradients. The program allows for the reattachment of the flow and continuation of the calculations for turbulent flow, if this is desired. As discussed previously, the user can also force transition to turbulent flow at any station, including the inlet.

ANALYTICAL LOSS CHARACTERISTICS

The displacement and momentum thicknesses at the blade exit (stator and rotor) can be used to calculate the aftermixing conditions downstream of the blade row assuming that the flow mixes to a uniform state. Application of the continuity, momentum, and energy equations results in the determination of the aftermixing Mach number, flow angle, pressure ratio, and kinetic energy loss. The calculation procedure has been described in (12). The mixing losses obtained in this manner are for two-dimensional blade rows. A method of estimating three-dimensional losses from two-dimensional losses is given in (13).

Subsonic and supersonic aftermixing axial Mach number solutions are possible for this loss model when the free-stream axial Mach number at the blade exit (before mixing) is supersonic. As discussed in (14), the subsonic axial Mach number solution corresponds to mixing plus oblique shock losses, whereas the supersonic axial Mach number solution corresponds to shockless mixing. As indicated in (14), the supersonic solution may not be physically possible in a turbine unless there is an increase in the annulus area.

Stator Blade Efficiency

The analytical stator blade efficiency is defined as

$$\eta_n = \left(\frac{V_2}{V_{2,id}}\right)^2 \qquad (1)$$

where V_2 is the stator aftermixing velocity, and $V_{2,id}$ is the ideal velocity obtained by isentropic expansion to the stator aftermixing static pressure. The analytical stator blade efficiency as a function of stator flow angle is shown in figure 3 for stators designed for a free-stream Mach number of 3.5. As expected, the efficiency for the supersonic solution is higher than for the subsonic solution because of the absence of shock losses for the supersonic solution. For the subsonic solution, as the flow angle α_1 decreases the oblique shock across the exit plane approaches a normal shock, resulting in a large decrease in efficiency. The aftermixing Mach number, flow angle, and pressure ratio, as well as the results for different Mach number levels can be found in (14). The aftermixing conditions are also given as part of the output of the computer program for the stator design (3).

Rotor Blade Efficiency

The analytical rotor blade efficiency is defined as

$$\eta_R = \left(\frac{W_4}{W_{4,id}}\right)^2 \qquad (2)$$

where W_4 is the rotor aftermixing relative velocity, and $W_{4,id}$ is the ideal relative velocity obtained by isentropic expansion to the rotor aftermixing static pressure. The analytical efficiency as a function of lower- and upper-surface Mach number is shown in figure 4 for rotors designed for a relative inlet Mach number of 2.5. Since a low Reynolds number example was chosen, two cases were considered: (1) laminar separation with reattachment (the momentum thickness before and after separation being assumed equal) and, (2) turbulent flow forced at the inlet. The laminar separation model gives larger blade losses because the laminar portion of the calculations results in larger momentum thicknesses as compared with the corresponding turbulent calculation. The blade efficiency increases when either the lower-surface Mach number decreases or the upper-surface Mach number increases. This is expected since these changes increase the passage width which results in a smaller percentage of the passage being occupied by the boundary layer. These results assumed that the turbulent boundary layer does not separate. The problems associated with decreasing the lower-surface Mach number or increasing the upper-surface Mach number is discussed in the next section.

The aftermixing Mach numbers, flow angles, and pressure ratios, corresponding to this example can be found in (15). The aftermixing conditions are also part of the output of the computer program for the rotor design (4).

DESIGN LIMITATIONS

Decreasing the lower-surface Mach number or increasing the upper-surface Mach number tends to increase the rotor blade efficiency. While this is desirable, other factors such as flow separation, blade solidity, and supersonic starting must be considered before a blade design is selected.

Flow Separation

For the laminar boundary layer calculations, the computer program will generally predict separation for fairly small adverse pressure gradients. This was

discussed previously. For turbulent boundary layers, the calculations also give an indication whether flow separation will occur. This information is obtained from the distribution of the incompressible form factor H_i along the blade surfaces. A typical distribution of H_i and the corresponding surface Mach number distribution is shown in figure 5. Turbulent separation usually occurs for values of H_i from 1.8 to 2.4 (16). It is seen that turbulent separation is possible on both the lower- and upper-surfaces of the blade. Separation on the lower-surface, if it occurs, is probably not as important since the flow would tend to reattach shortly downstream. The maximum value of H_i along either surface generally occurs at the end point (point I and F of fig. 5) of the transition arc.

The effect of the lower- and upper-surface Mach number on the maximum value of the incompressible form factor H_i is shown in figure 6. The maximum value of H_i increases (the probability of separation increases) when either the lower-surface Mach number decreases or the upper-surface Mach number increases. These same changes in surface Mach number were previously found to increase the rotor blade efficiency. An optimum rotor blade design would therefore be expected to occur for a blade in which the lower- and upper-surface Mach numbers are chosen such that turbulent separation is imminent on each surface.

Blade Solidity

The effect of the lower- and upper-surface Mach number on blade solidity is shown in figure 7. The solidity decreases as the lower-surface Mach number decreases or the upper-surface Mach number increases. For a constant blade chord, this means that the number of blades decrease, which is desirable from practical considerations. However, these trends in surface Mach number increase the probability of turbulent separation.

Supersonic Starting

The mechanism by which supersonic flow is established within the rotor passage must be known if the blade sections are to be designed properly. It is usually assumed (10) that a normal shock wave spans the rotor blade entrance at the instant of starting. The passage must therefore be designed large enough to permit the shock to pass through, if supersonic flow is to be established. For given surface Mach numbers, which fixes the amount of passage contraction, there exists a maximum value of the inlet Mach number for which supersonic flow can be established. The maximum inlet Mach number $M_{r,2}$ as a function of the lower- and upper-surface Mach numbers is shown in figure 8. Increasing the lower- and upper-surface Mach number increases the maximum value of the inlet Mach number, which is desirable from starting considerations. However, increasing the upper-surface Mach number tends to increase the probability of flow separation. A compromise between these opposing tendencies must sometimes be made in an actual design. It should be emphasized that the supersonic starting restriction applies only if a normal shock is present at the instant of starting. In some cases this restriction may not be fully applicable as indicated by the experimental investigation presented in (17).

EXPERIMENTAL PERFORMANCE

The experimental performance of a single-stage partial admission supersonic turbine operating at a low Reynolds number is presented in this section. A brief description of the apparatus and the test procedure is also given. Further details on the experimental work can be found in (5).

General Turbine Design Characteristics

The turbine was aerodynamically designed to operate using hydrogen-oxygen combustion products at a turbine inlet temperature of 1389 K (2500 R) and a mean blade speed of 731.5 m/sec (2400 ft/sec). The specific heat ratio was 1.356. The turbine was tested using room temperature air at equivalent design conditions which were:

Specific work,
$\Delta h/\theta_{cr}$ . . . . . 10.56×10^4 J/kg (45.44 Btu/lb)
Mean blade speed,
$Um/\sqrt{\theta_{cr}}$ . . . . . 136.9 m/sec (449.0 ft/sec)
Mass flow,
$w\sqrt{\theta_{cr}}\ \varepsilon/\delta$ . . . . . 0.00336 kg/sec (0.00739 lb/sec)
Pressure ratio, p_o'/p_4 63

The turbine had a mean diameter of 0.218 m (8.6 in.) and a hub-tip radius ratio of 0.923. The admission was 9.2% and the design air Reynolds number Re was approximately 75 000 based on blade height. The velocity diagram is shown in figure 9.

The stator was designed, by the method described previously, for a free-stream Mach number before mixing of 3.65. The subsonic axial Mach number solution was used for the mixing calculations and resulted in a 12% loss in total pressure. The aftermixing Mach number was 2.85. The stator which consisted of two nozzles, whose throat dimension was 0.112 cm (0.044 in.), is shown in figure 10.

The rotor was designed, by the method described previously, assuming a turbulent boundary layer at the inlet. It was recognized that the boundary layer was probably laminar (because of the low Reynolds number) but the laminar separation and reattachment option was not available at the time of the design. The rotor was designed for a lower- and upper-surface Mach number level of 1.75 and 2.38, respectively. The aftermixing calculations resulted in a calculated turbine static efficiency of 50%. The rotor which consisted of 170 blades, whose solidity was 3.2, is shown in figure 11.

Apparatus and Instrumentation

The apparatus used for the investigation consisted of a single-stage turbine, a flywheel to absorb the power output of the turbine, and an inlet and outlet piping system. A sketch of the turbine assembly is shown in figure 12. The turbine shaft was vertical, stationary, and hollow to facilitate cooling of the solid lubricated bearings.

The turbine assembly was enclosed in a vacuum tank that connected into a low-pressure exhaust system. Pressurized air, which was dried and filtered, passed through a pressure regulator before entering the stator. The stator was choked for all test conditions investigated and was flow calibrated prior to installation. After leaving the turbine, the air was exhausted into the low-pressure exhaust system. With a fixed exhaust pressure, the inlet pressure was remotely regulated to obtain the desired pressure ratio across the turbine.

The turbine was instrumented so that over-all

turbine performance data could be obtained. Pressures were measured at the turbine inlet and in the vacuum tank. Temperatures were measured at the turbine inlet and on the bearing inner races. The rotational speed of the turbine was obtained by use of a Hall generator in conjunction with a small magnet embedded in the flywheel. Rotation of the flywheel caused a series of pulses to be generated by the Hall crystal, with the frequency of the pulses being proportional to the rotational speed of the turbine.

Procedure

The experimental tests were conducted by operating the turbine at constant pressure ratios. The inlet pressure was regulated to obtain the desired pressure ratio. The turbine speed was allowed to vary from zero to slightly over equivalent design speed, at which point the air flow to the turbine was terminated. During the acceleration and deceleration of the turbine the speed variation was recorded. The inertia of the flywheel was selected so that the turbine accelerated to the design speed in a few minutes.

The static efficiency η_s was obtained from

$$\eta_s = \frac{\Delta h}{C_p T_o' \left\{ 1 - \left(\frac{p_4}{p_o'} \right)^{(\gamma-1)/\gamma} \right\}} \tag{3}$$

where p_4/p_o' is the static-to-total pressure ratio across the turbine. The specific work Δh was calculated from the relation

$$\Delta h = \frac{\tau \omega}{w} \tag{4}$$

and the torque τ from

$$\tau = I \frac{d\omega}{dt} \tag{5}$$

The moment of inertia I of the rotating assembly was determined experimentally. The turbine acceleration rate $d\omega/dt$ was obtained from the turbine speed versus time plot. A typical plot is shown in figure 13 and consists of two regions: (1) an accelerating region in which the turbine is producing work over and above that lost due to bearing friction and windage, and (2) a deceleration region in which the turbine is producing no work (zero flow); the deceleration being caused by the bearing friction and windage losses. The turbine acceleration rate $d\omega/dt$ was calculated from

$$\frac{d\omega}{dt} = m_{acc} - m_{dec} \tag{6}$$

where m_{acc} and m_{dec} are the slopes of the speed versus time curve in the accelerating and decelerating regions, respectively. In effect, this procedure does not take into account the windage losses. In other words, the experimental efficiency presented herein is the efficiency level that would be obtained from the turbine if it operated with zero windage losses. In certain space applications, where the turbine would operate in a hard vacuum, the windage losses would be negligible. In other situations, the windage losses must be charged to the turbine.

Stator Pressure Distribution

The pressure distribution of the stator was measured prior to testing the turbine. Static pressure taps were located along the divergent and straight section of the nozzle to obtain these measurements. For the full turbine tests the nozzles were not instrumented.

The pressure distribution in the nozzle was obtained at design and off-design conditions and is shown in figure 14. At the design pressure ratio, the agreement between theory and experiment is good for the divergent portion of the nozzle. Along the straight section, where the pressure should be theoretically constant, the pressure first decreases below design and then increases. This behavior which is apparently caused by expansion and shock waves forming on the straight section, would be expected to adversely affect rotor performance if it persisted in the full turbine. Typical nozzle off-design behavior is seen to occur at higher than design static-to-total pressure ratios, with the pressure increasingly sharply within the nozzle due to shock wave formation.

Turbine Efficiency

The static efficiency η_s is shown in figure 15 as a function of blade-jet speed ratio for constant speeds. The total-to-static pressure ratio was varied from 20 to 150 while the speed varied from 20 to 100 percent of design. As explained in the Procedure Section, the experimental efficiency presented in figure 15 is the efficiency that would be obtained if the turbine operated with zero windage losses. Since the other partial admission losses (i.e., expansion and filling losses) are estimated to be small, a comparison between the experimental and the analytical results (which have not been corrected for partial admission losses) is permissible. For design pressure ratio and speed the static efficiency was 0.39 which is 11 percentage points lower than the analytically predicted value.

A number of possible explanations are offered for this discrepancy. The nozzle performance, which was shown to deviate from design (because of apparent shock formation) would tend to decrease the turbine efficiency. This would result from an adverse effect on the rotor performance and also possibly from increased turbine leaving losses. As indicated previously, the design procedure was based on boundary layer calculations which were assumed turbulent throughout the rotor. A laminar boundary layer would give higher rotor blade losses, as would separation of the flow. The measured efficiency level, however, is in reasonable agreement with that obtained from a similar type of turbine (17).

The maximum efficiency obtained at any fixed speed occurred at or near the design pressure ratio. The rapid drop-off of the efficiency at off-design pressure ratio is typical of supersonic turbines and similar to trends found in reference (18).

CONCLUDING REMARKS

Methods for designing supersonic stator and rotor blading corrected for boundary layer displacement thickness are summarized. Computer programs based on these methods have been reported in references (3) and (4). Analytical blade losses for blading of this type are presented and design limitations resulting from consideration of flow separation

and supersonic starting are discussed. The experimental performance of a single-stage turbine designed by these methods and reported in (5) is also summarized.

The experimental results indicated a turbine efficiency level well below that predicted analytically. A number of sources of additional losses not accounted for in the design method, including shock losses, laminar boundary layer losses and flow separation are offered as a possible explanation for this discrepancy. More work is necessary in order to better identify these losses so that they may be incorporated in the design method.

REFERENCES

1 Vanco, M. R., "Thermodynamic and Turbine Characteristics of Hydrogen-Fueled Open-Cycle Auxiliary Space Power Systems," TM X-1337, 1967, NASA, Cleveland, Ohio.

2 Fruchtman, I., "The Supersonic Turbine - A Design and Cascade Study," Paper 71-GT-76, Mar. 1971, ASME, New York, N.Y.

3 Goldman, L. J., and Vanco, M. R., "Computer Program for Design of Two-Dimensional Sharp-Edged-Throat Supersonic Nozzle with Boundary-Layer Correction," TM X-2343, 1971, NASA, Cleveland, Ohio.

4 Goldman, L. J., and Scullin, V. J., "Computer Program for Design of Two-Dimensional Supersonic Rotor Blades with Boundary Layer Correction," proposed Technical Memorandum, NASA, Cleveland, Ohio.

5 Goldman, L. J., "Experimental Investigation of a Low Reynolds Number Partial-Admission Single-Stage Supersonic Turbine," TM X-2382, 1971, NASA, Cleveland, Ohio.

6 Vanco, M. R., and Goldman, L. J., "Computer Program for Design of Two-Dimensional Supersonic Nozzle with Sharp-Edged Throat," TM X-1502, 1968, NASA, Cleveland, Ohio.

7 McNally, W. D., "FORTRAN Program for Calculating Compressible Laminar and Turbulent Boundary Layers in Arbitrary Pressure Gradients," TN D-5681, 1970, NASA, Cleveland, Ohio.

8 Cohen, C. B., and Reshotko, E., "The Compressible Laminar Boundary Layer with Heat Transfer and Arbitrary Pressure Gradient," TR 1294, 1956, NACA, Cleveland, Ohio.

9 Sasman, P. K., and Cresci, R. J., "Compressible Turbulent Boundary Layer with Pressure Gradient and Heat Transfer," AIAA Journal, Vol. 1, No. 4, Jan. 1966, pp. 19-25.

10 Boxer, E, Sterrett, J. R., and Wlodarski, J., "Application of Supersonic Vortex-Flow Theory to the Design of Supersonic Impulse Compressor- or Turbine-Blade Sections," RM L52B06, 1952, NACA, Hampton, Va.

11 Goldman, L. J., and Scullin, V. J., "Analytical Investigation of Supersonic Turbomachinery Blading. I - Computer Program for Blading Design," TN D-4421, 1968, NASA, Cleveland, Ohio.

12 Stewart, W. L., "Analysis of Two-Dimensional Compressible-Flow Loss Characteristics Downstream of Turbomachinery Blade Rows in Terms of Basic Boundary-Layer Characteristics," TN 3515, 1955, NACA, Cleveland, Ohio.

13 Stewart, W. L., Whitney, W. J., and Wong, R. Y., "Use of Mean-Section Boundary-Layer Parameters in Predicting Three-Dimensional Turbine Stator Losses," RM E55L12a, 1956, NACA, Cleveland, Ohio.

14 Goldman, L. J., and Vanco, M. R., "Analytical Investigation of Two-Dimensional Loss Characteristics of Supersonic Turbine Stator Blades," TM X-1823, 1969, NASA, Cleveland, Ohio.

15 Goldman, L. J., "Analytical Investigation of Blade Efficiency for Two-Dimensional Supersonic Turbine Rotor Blade Sections," TM X-2095, 1970, NASA, Cleveland, Ohio.

16 Schlichting, H (J. Kestin, trans.), Boundary-Layer Theory, 6th ed., McGraw-Hill, New York, 1968.

17 Moffitt, T. P., "Design and Experimental Investigation of a Single-Stage Turbine with a Rotor Entering Relative Mach Number of 2," RM E58F20a, 1958, NACA, Cleveland, Ohio.

18 Moffitt, T. P., and Klag, F. W., Jr., "Experimental Investigation of Partial- and Full-Admission Characteristics of a Two-Stage Velocity-Compounded Turbine," TM X-410, 1960, NASA, Cleveland, Ohio.

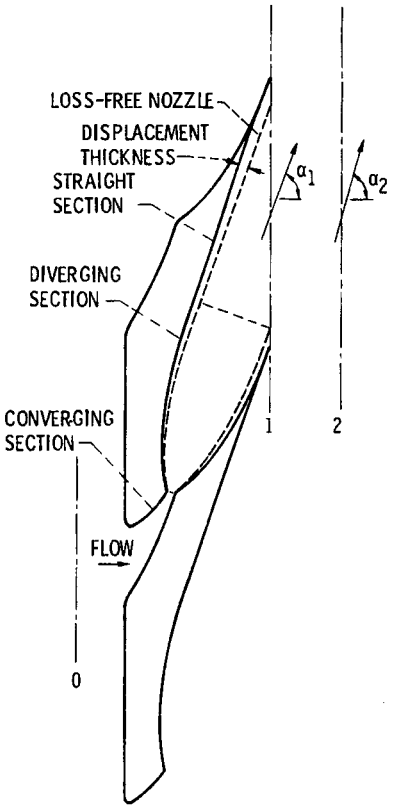

Figure 1. - Supersonic nozzle design.

AB AND FG	STRAIGHT LINES
BC AND EF	UPPER TRANSITION ARCS
HI AND KL	LOWER TRANSITION ARCS
CDE AND IJK	CIRCULAR ARCS

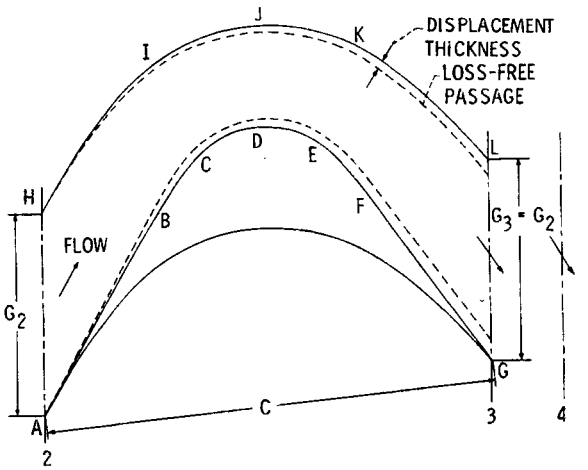

Figure 2. - Supersonic rotor design.

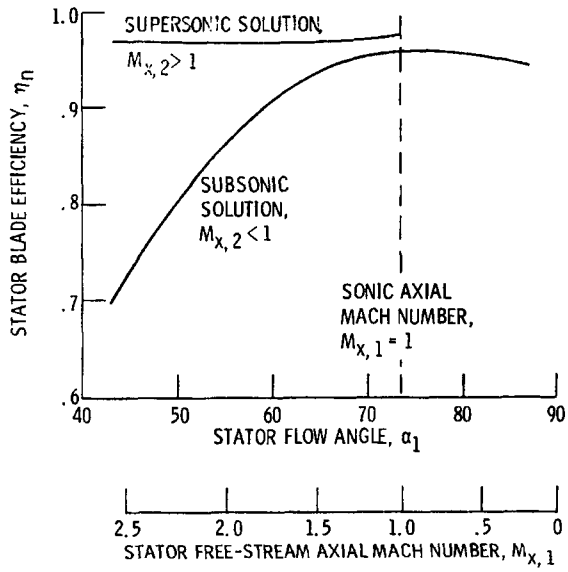

Figure 3. - Analytical stator blade efficiency, $M_{fs,1} = 3.5$, $Re_t = 10\,000$, $\gamma = 1.4$.

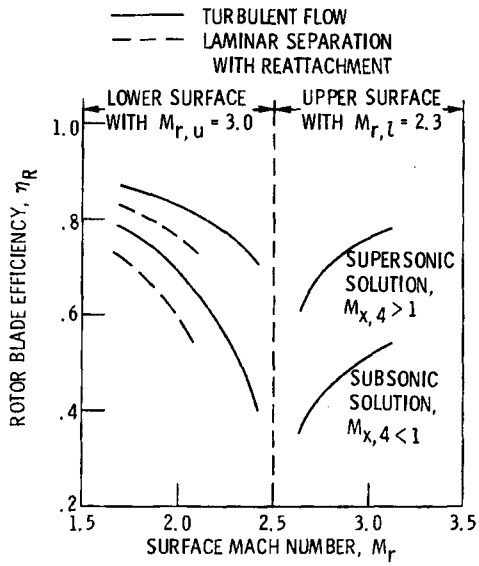

Figure 4. - Analytical rotor blade efficiency, $M_{r,2} = 2.5$, $Re_R = 35\,000$, $\gamma = 1.4$.

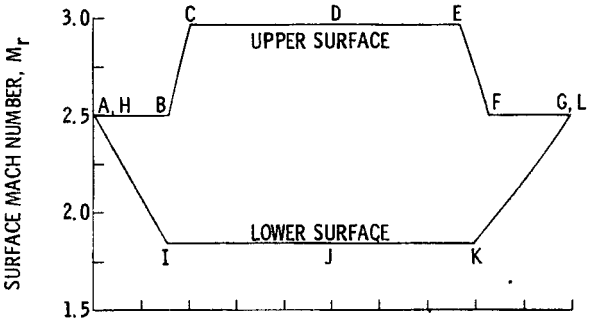

(b) MACH NUMBER.

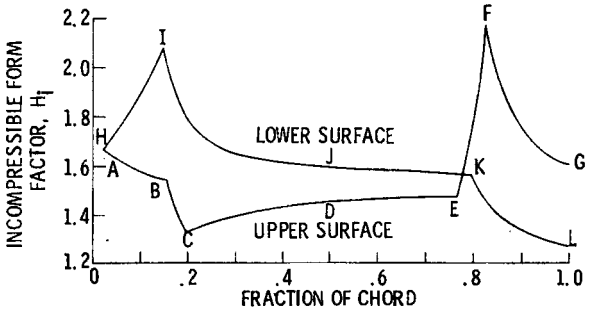

(a) FORM FACTOR.

Figure 5. - Distribution of form factor and Mach number for typical rotor blade.

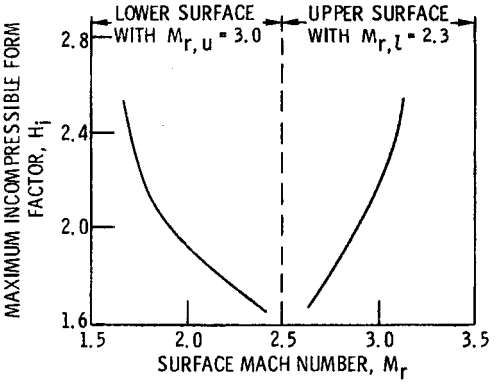

Figure 6. - Effect of surface Mach number on form factor.

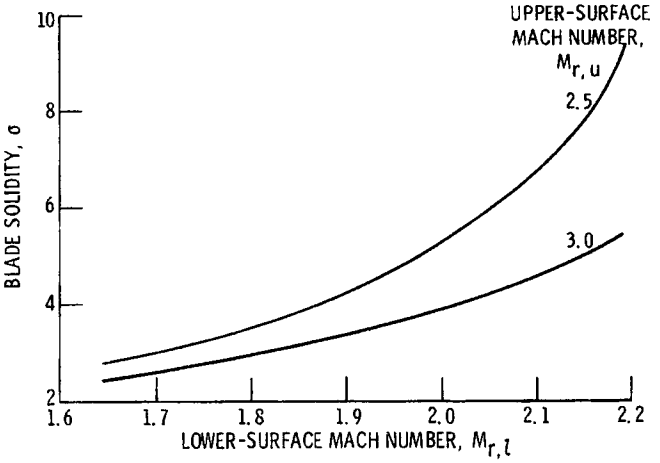

Figure 7. - Effect of surface Mach numbers on blade solidity, $M_{r,2}$ = 2.5, γ = 1.4.

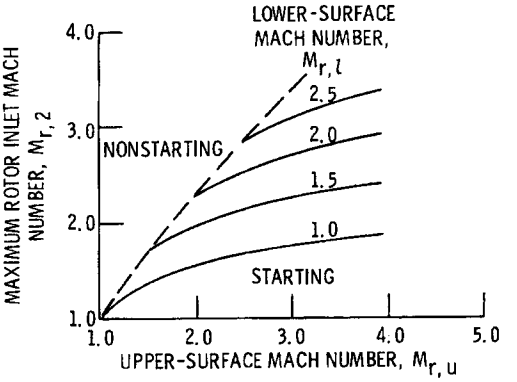

Figure 8. - Maximum rotor inlet Mach number for supersonic starting, γ = 1.4.

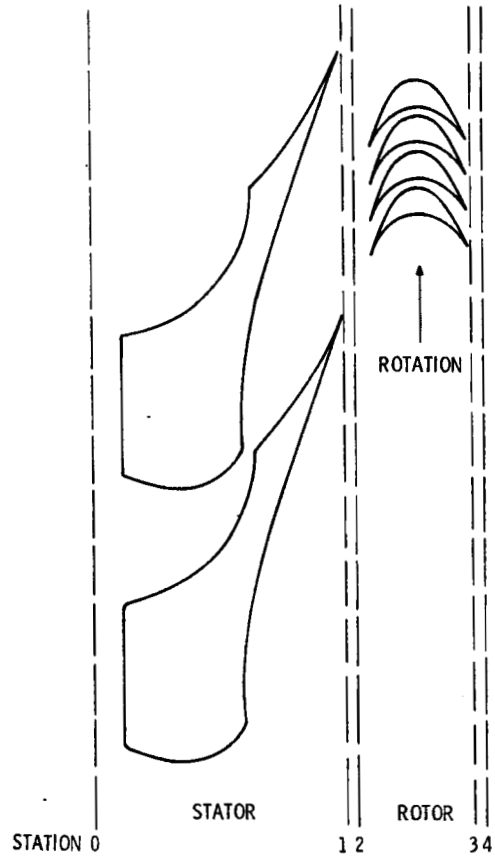

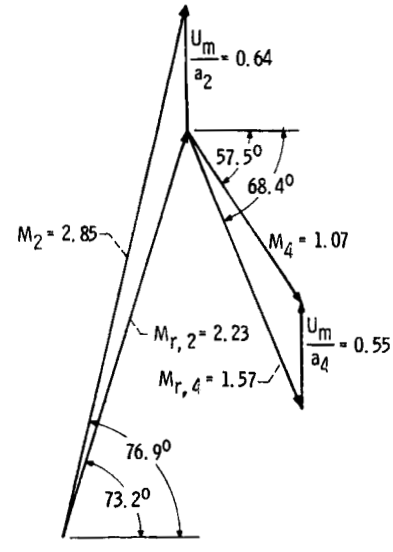

Figure 9. - Turbine design velocity diagram.

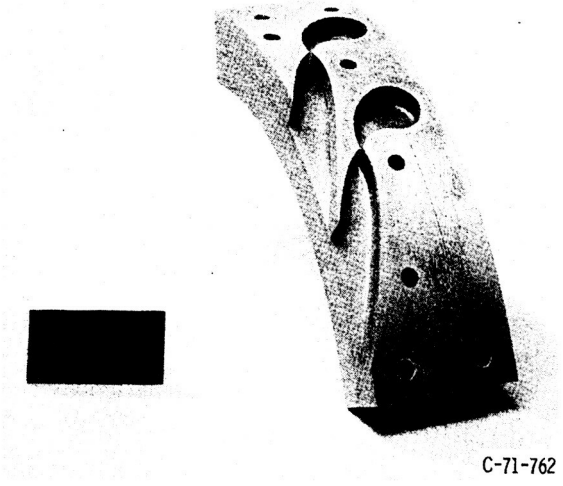

Figure 10. - Stator.

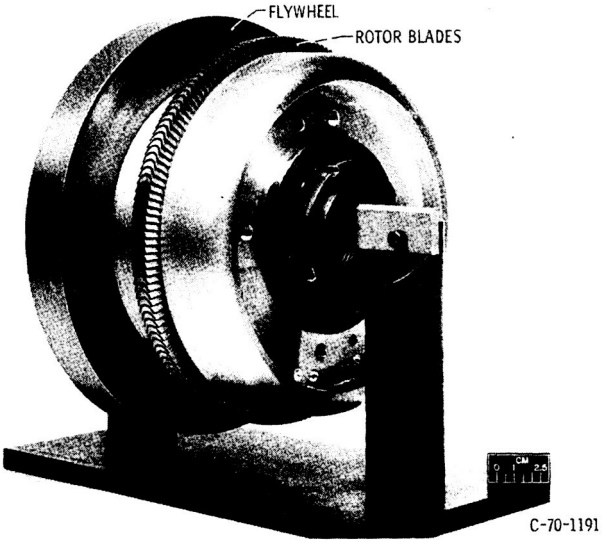

Figure 11. - Rotor.

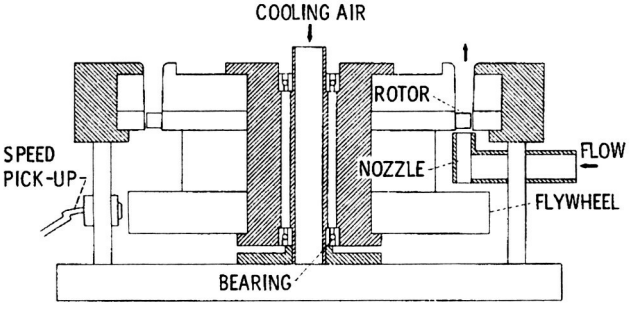

Figure 12. - Cross-sectional view of supersonic turbine.

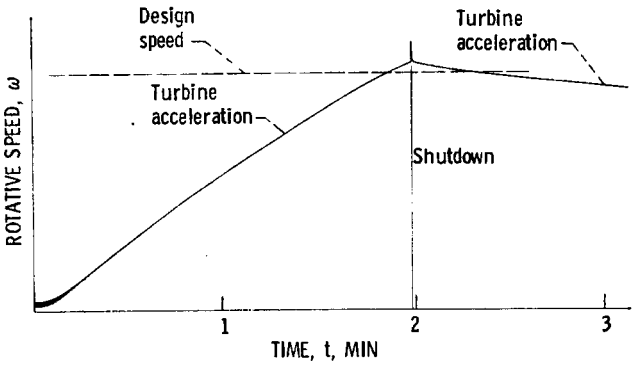

Figure 13. - Typical turbine speed variation during test.

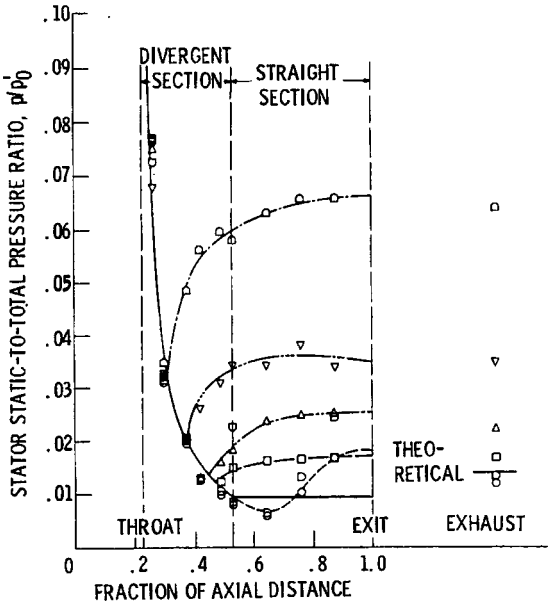

Figure 14. - Stator pressure distribution.

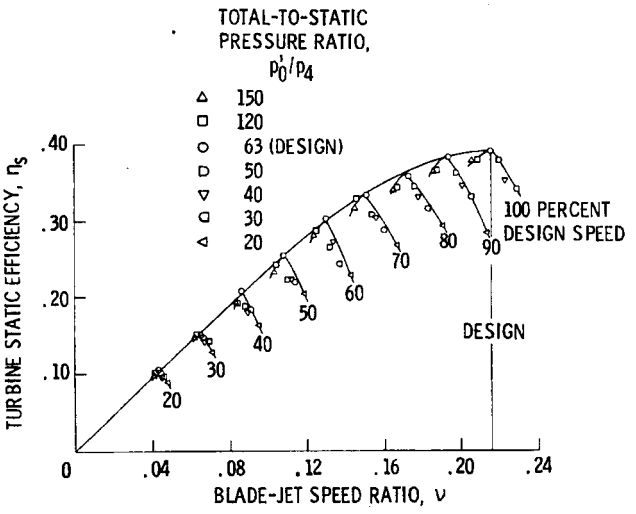

Figure 15. - Turbine efficiency versus blade-jet speed ratio.